De Rosario Martínez, H.; Page Del Pozo, AF.; Besa Gonzálvez, AJ. (2017). Analytical study of the effects of soft tissue artefacts on functional techniques to define axes of rotation. Journal of Biomechanics. 62:60-67. doi:10.1016/j.jbiomech.2017.01.046

Analytical study of the effects of soft tissue artefacts on functional techniques to define axes of rotation

Helios De Rosario, Álvaro Page, Antonio Besa

PII: S0021-9290(17)30080-5
DOI: http://dx.doi.org/10.1016/j.jbiomech.2017.01.046
Reference: BM 8118

To appear in: *Journal of Biomechanics*

Accepted Date: 27 January 2017

Please cite this article as: H.D. Rosario, A. Page, A. Besa, Analytical study of the effects of soft tissue artefacts on functional techniques to define axes of rotation, *Journal of Biomechanics* (2017), doi: http://dx.doi.org/10.1016/j.jbiomech.2017.01.046

Analytical study of the effects of soft tissue artefacts on functional techniques to define axes of rotation

Helios De Rosario [a,b,*], Álvaro Page [a,b], Antonio Besa [c]

[a] *Instituto de Biomecánica de Valencia, Valencia, Spain*

[b] *CIBER de Bioingeniería, Biomateriales y Nanomedicina (CIBER-BBN), Spain*

[c] *Centro de Investigación en Ingeniería Mecánica, Universitat Politècnica de València, Valencia, Spain*

* Corresponding author: Instituto de Biomecánica de Valencia, Universitat Politècnica de València, Edificio 9C, Camino de Vera s/n, E-46022, Valencia, Spain.

Tel: +34 961111170. Fax: +34 963879169.

E-mail: helios.derosario@ibv.upv.es

Keywords: Functional Calibration, Axis of Rotation, Soft Tissue Artefacts, Geometric Fitting, Finite Helical Axis, Knee Joint

Word count (Introduction through Discussion): 3,515

Number of tables: 3

Number of figures: 5

Abstract

The accurate location of the main axes of rotation (AoR) is a crucial step in many applications of human movement analysis. There are different formal methods to determine the direction and position of the AoR, whose performance varies across studies, depending on the pose and the source of errors. Most methods are based on minimizing squared differences between observed and modelled marker positions or rigid motion parameters, implicitly assuming independent and uncorrelated errors, but the largest error usually results from soft tissue artefacts (STA), which do not have such statistical properties and are not effectively cancelled out by such methods. However, with adequate methods it is possible to assume that STA only account for a small fraction of the observed motion and to obtain explicit formulas through differential analysis that relate STA components to the resulting errors in AoR parameters. In this paper such formulas are derived for three different functional calibration techniques (Geometric Fitting, mean Finite Helical Axis, and SARA), to explain why each technique behaves differently from the others, and to propose strategies to compensate for those errors. These techniques were tested with published data from a sit-to-stand activity, where the true axis was defined using bi-planar fluoroscopy. All the methods were able to estimate the direction of the AoR with an error of less than 5º, whereas there were errors in the location of the axis of 30 to 40 mm. Such location errors could be reduced to less than 17 mm by the methods based on equations that use rigid motion parameters (mean Finite Helical Axis, SARA) when the translation component was calculated using the three markers nearest to the axis.

Table of symbols

$\delta x, \delta \mathbf{x}$	Error in the quantity x or the vector $\mathbf{x}$ due to soft tissue artefacts.
$\delta\theta$	Angle between theoretical and measured finite helical axis or axis of rotation
θ_i	Amount of rotation associated to a rigid motion at time t_i.
$\delta\varphi_i$	Amount of rotation observed in a marker cluster due to soft tissue artefacts at time t_i.
$\mathbf{d}_{Oi}$	Translation component of a rigid motion measured at the origin of coordinates at time t_i.
$\mathbf{d}_{Ai}$	Translation component of a rigid motion measured at a point in the axis of rotation at time t_i.
$\mathbf{h}_A$	Point in the axis of rotation of a joint with fixed axis.
$\mathbf{h}_{Ai}$	Point in the finite helical axis of a rigid motion at time t_i.
$\mathbf{n}$	Unit vector defining the direction of the axis of rotation in a joint with fixed axis.
$\mathbf{n}_i$	Unit vector defining the direction of the finite helical axis of a rigid motion at time t_i.
$\mathbf{p}_0$	Vector perpendicular to the finite helical axis of a rigid motion, going from that axis to an arbitrary fixed point of moving body (e.g. the centre of the marker cluster in the reference position).
$q_{iw}, \mathbf{q}_{iv}$	Scalar and vector components of the quaternion associated to a 3-D rotation at time t_i.
$\mathbf{r}_{ji}$	Position of marker j in the global coordinate system at time t_i.
$\mathbf{s}_{ji}$	Difference between the position of marker j at time t_i ($\mathbf{r}_{ji}$) and its average

position through all the measurement.

$\mathbf{u}_i$ Direction of the finite helical axis associated to the rigid component of soft tissue artefacts in a marker cluster at time t_i.

1. Introduction

Reconstructing joint kinematics requires the accurate definition of anatomical axes, which in some joints are determined by the main direction of rotation. Functional calibration techniques to determine the axes of rotation (AoR) are preferred to regression methods when the joint has an adequate range of motion or when the precise location of anatomical landmarks is difficult, as is the case in the knee joint (Besier et al., 2003; Della Croce et al., 2005).

There are different mathematical methods for calculating the AoR from observed marker positions, which can be broadly classified as 'transformation' and 'fitting' techniques (Ehrig et al., 2007). Transformation techniques are based on characterising marker clusters as rigid bodies associated with moving coordinate systems and calculating a common axis for the ensemble of observed postures. This was first proposed by Woltring (1990) as a procedure for 'averaging' instantaneous helical axes. But many authors have preferred to use finite helical axes (FHA), which are associated with rotations between pairs of separated poses, thus avoiding the amplification of errors at low velocities (Camomilla et al., 2006; Schwartz and Rozumalski, 2005). The 'symmetrical AoR approach' (SARA) proposed by Ehrig et al. (2007) is a particularly effective alternative for compensating for errors when the markers of both moving segments experiment relative motions (Colle et al., 2016; Reichl and Ongaro, 2013).

On the other hand, fitting techniques look for the axis that provides the best fit of marker positions to circular or cylindrical trajectories around it, without assuming rigid motions (Halvorsen et al., 1999). The geometric fitting method proposed by Gamage and Lasenby (2002) has been reported to be particularly effective for finding the AoR of the knee (MacWilliams, 2008; Van Campen et al., 2011).

There is no definitive consensus about which technique is most effective. Most comparisons have been made with simulated random noise or mechanical analogues. The few studies that contain *in-vivo* measurements give conflicting results in favour of either GF (Van Campen et al., 2011) or SARA (Colle et al., 2016). However, such apparent contradictions could be explained by differences in the characteristics of subjects and experimental procedures, and the influence of the calculation method itself remains unclear.

Soft-tissue artefacts (STA) are another relevant factor, since they are a major cause of errors in human movement analysis and of disparities between studies using different subjects and tasks (Lin et al., 2016). STA have a complex nature; they are correlated with bone motion and operate at the level of both individual markers and the whole cluster. However, each functional calibration technique implies different assumptions about the statistical properties of errors, marker cluster kinematics, and relationships between the motion of linked segments.

Thus, a better understanding of how STA interact with the kinematic analysis underlying functional calibration techniques may be useful to ascertain how errors can be compensated for more effectively. In this work we therefore present a mathematical model of STA propagation to the position and direction of variable and fixed axes, as calculated by three methods: mean FHA (MFHA, Woltring et al., 1985; Woltring, 1990), SARA (Ehrig et al., 2007), and geometric fitting (GF, Gamage and Lasenby, 2002), based on analysis of the equations used by those methods. This approach was previously used to gain insight into how errors are propagated to centres of rotation, comparing the resulting equations with data measured with a mechanical analogue (De Rosario et al., 2013). In this work we propose similar models for fixed axes, and

evaluate the effectiveness of different STA-compensation strategies deriving from them, using *in-vivo* data from published research.

2. Methods

2.1. Mathematical conventions

We describe joint motion as a relative movement between two segments, expressed in a coordinate system that is fixed in one of them. At each instant t_i $(i = 1,2,...,N)$, the pose of the moving bone is defined w.r.t. a reference pose by the translation of the origin of its coordinate system $(\mathbf{d}_{Oi})$, plus a rotation θ_i around the unit vector $\mathbf{n}_i$. To abbreviate the formulas, rotations are defined as quaternions with a real part $q_{iw} = \cos(\theta_i / 2)$ and an imaginary vector $\mathbf{q}_{iv} = \sin(\theta_i / 2)\mathbf{n}_i$. The FHA is defined as a line oriented as $\mathbf{n}_i$, passing through a point A_i whose position is $\mathbf{h}_{Ai}$ (figure 1).

The moving segment is observed through a set of skin markers P_j $(j = 1,2,...,M)$. We use the vectors $\mathbf{r}_{ji}$ to represent the theoretical 'error-free' marker positions, and $\delta\mathbf{r}_{ji}$ for the superimposed STA, which we assume to be small $\left(\left|\mathbf{r}_{ji} - \mathbf{r}_{j0}\right| >> \left|\delta\mathbf{r}_{ji}\right|\right)$. In the following sections we present the equations that define how those STA determine the orientation and position errors of the FHA at each instant $(\delta\mathbf{n}_i, \delta\mathbf{h}_{Ai})$, as well as those of the fixed AoR estimated by GF, MFHA and SARA.

2.2. Propagation of STA to a variable FHA

STA exhibit two clearly differentiated components: a deformation due to relative displacements of individual markers, and the collective rigid movement of the cluster, which has the greatest impact on kinematic analysis (Bonci et al., 2015; De Rosario et

al., 2012; Dumas et al., 2015). That rigid component of STA can be characterised as a small rotation $\delta\varphi_i$ around the axis $\mathbf{u}_i$, and the translation $\delta\mathbf{p}_i$ of a known fixed point (e.g. the centre of the marker cluster), which in the reference pose is located at a point separated by the vector $\mathbf{p}_0$ from the AoR (figure 1). As explained in the supplementary material, we can estimate errors of FHA orientation and position as follows:

The angle $\delta\alpha_i$ between theoretical and measured FHA can be approximated as:

$$\delta\alpha_i = \frac{\delta\varphi_i\left(1 - \mathbf{u}_i \cdot \mathbf{n}_i\right)}{2\sin\left(\theta_i/2\right)} \qquad (1)$$

The position error of the FHA $\delta\mathbf{h}_{Ai}$ has four terms:

$$\delta\mathbf{h}_{Ai} = \frac{\mathbf{n}_i \times \delta\mathbf{p}_i}{2\tan\left(\theta_i/2\right)} - \frac{1}{2}\mathbf{n}_i \times \left(\mathbf{n}_i \times \delta\mathbf{p}_i\right) - \frac{\delta\theta_i}{2\tan\left(\theta_i/2\right)}\mathbf{p}_0 + \frac{\delta\theta_i}{2}\left(\mathbf{n}_i \times \mathbf{p}_0\right) \qquad (2)$$

where the error of the rotation angle $\delta\theta_i$ is the projection of the rotation artefact on the direction of the FHA:

$$\delta\theta_i = \delta\varphi_i \mathbf{u}_i \cdot \mathbf{n}_i \qquad (3)$$

It may be noted that all the terms of $\delta\mathbf{h}_{Ai}$ related to rotation errors are proportional to $\left|\mathbf{p}_0\right|$.

2.3. Propagation of STA to fixed AoR

The methods used to calculate fixed AoR and the error formulas derived from them are described in the supplementary material, with a homogeneous formulation derived from the definitions given in the original papers. All functional calibration techniques define the direction and position of the AoR $\left(\mathbf{n}, \mathbf{h}_A\right)$ by matrix equations of the type $A\mathbf{h}_A = \mathbf{b}$, where both $A, \mathbf{b}$ depend on the specific method. In all cases A is an ill-conditioned

matrix, and the problem is solved by singular value decomposition: the singular vector associated with the smallest singular value represents the AoR direction $\mathbf{n}$, and a stable value of $\mathbf{h}_A$ is obtained from a reduced 2-D system of equations, considering the projections of $A, \mathbf{b}$ onto the two main axes obtained by the singular value decomposition.

To facilitate the analysis we considered that all vectors are expressed in an 'axial coordinate system' (ACS), with coordinate axes equal to the singular vectors obtained by singular value decomposition, such that the AoR is the *Z*-axis and the origin is a point A on the AoR. The quaternion that represents the rotation of the bone in the ACS is $q_{iw} = \cos(\theta_i / 2), \mathbf{q}_{iv} = [0,0,\sin(\theta_i / 2)]$; and its error due to STA can be derived from the following formulas using the amount of rotation associated to the STA — as explained in the supplementary material:

$$\delta q_{iw} = -\frac{\delta\phi_i}{2}\mathbf{q}_{iv}\mathbf{u}_i \tag{4}$$

$$\delta\mathbf{q}_{iv} = [\delta q_{iX} \quad \delta q_{iY} \quad \delta q_{iZ}] = \frac{\delta\phi_i}{2}(q_{iw}\mathbf{u}_i + \mathbf{q}_{iv} \times \mathbf{u}_i) \tag{5}$$

The error propagated to AoR parameters is estimated as follows:

The orientation error is expressed as two small rotations around the first and second axes of the ACS, $\delta\alpha_X$, $\delta\alpha_Y$. For MFHA and GF, the value of these angles is a weighted average of rotation and marker position errors ($\delta q_{iX,Y,Z}$ and $\delta\mathbf{r}_{ji}$, respectively):

$$\delta\alpha_{X\,MFHA} = -\frac{\sum_i q_{iZ}\delta q_{iY}}{\sum_i q_{iZ}^2} \tag{6}$$

$$\delta\alpha_{Y\,MFHA} = \frac{\sum_i q_{iZ}\delta q_{iX}}{\sum_i q_{iZ}^2} \quad (7)$$

$$\delta\alpha_{X\,GF} = \frac{\sum_i \sum_j s_{jiY}\,\delta r_{jiZ}}{\sum_i \sum_j s_{jiY}^2} \quad (8)$$

$$\delta\alpha_{Y\,GF} = -\frac{\sum_i \sum_j s_{jiX}\,\delta r_{jiZ}}{\sum_i \sum_j s_{jiX}^2}, \quad (9)$$

where $\mathbf{s}_{ji} = \mathbf{r}_{ji} - \bar{\mathbf{r}}_j$ are the differences between $\mathbf{r}_{ji}$ and their average. Equations (6-7) assume that MFHA is applied with a weighting factor equal to $\sin^2(\theta_i/2)$, which is the optimal choice for reducing errors associated with small rotations (Ehrig et al., 2007).

The formulas for SARA are more involved, although can be reduced through the following abbreviations:

$$w = \sum_{i=1}^{N} q_{iw}^2$$

$$k = \frac{\sum_i q_{iw} q_{iZ}}{\sum_i q_{iw}^2}$$

Then:

$$\delta\alpha_{X\,SARA} = \frac{1}{N - w - wk^2}\left(-\sum_{i=1}^{N} q_{iZ}\delta q_{iY} + k\sum_{i=1}^{N} q_{iw}\delta q_{iY} \right) \quad (10)$$

$$\delta\alpha_{Y\,SARA} = \frac{1}{N - w - wk^2}\left(\sum_{i=1}^{N} q_{iZ}\delta q_{iX} - k\sum_{i=1}^{N} q_{iw}\delta q_{iX} \right) \quad (11)$$

The position error of the AoR can be expressed as a distance in the *XY* plane of the ACS. The errors with MFHA and SARA are proportional to the translation of the axis point A (A ∈ AoR) associated with STA $\left(\delta d_{AiX}, \delta d_{AiY}\right)$:

$$\delta h_{X\ MFHA} = \frac{1}{2}\left(\frac{\sum_i q_{iZ}^2 \delta d_{AiX}}{\sum_i q_{iZ}^2} - \frac{\sum_i q_{iw} q_{iZ} \delta d_{AiY}}{\sum_i q_{iZ}^2} \right) \quad (12)$$

$$\delta h_{Y\ MFHA} = \frac{1}{2}\left(\frac{\sum_i q_{iZ}^2 \delta d_{AiY}}{\sum_i q_{iZ}^2} + \frac{\sum_i q_{iw} q_{iZ} \delta d_{AiX}}{\sum_i q_{iZ}^2} \right) \quad (13)$$

$$\delta h_{X\ SARA} = \frac{1}{2\left(N - w - wk^2\right)}\left(\sum_{i=1}^{N} \left(q_{iZ}^2 - k q_{iw} q_{iZ}\right)\delta d_{AiX} - \sum_{i=1}^{N} \left(q_{iw} q_{iZ} - k q_{iw}^2\right)\delta d_{AiY} \right) \quad (14)$$

$$\delta h_{Y\ SARA} = \frac{1}{2\left(N - w - wk^2\right)}\left(\sum_{i=1}^{N} \left(q_{iZ}^2 - k q_{iw} q_{iZ}\right)\delta d_{AiY} + \sum_{i=1}^{N} \left(q_{iw} q_{iZ} - k q_{iw}^2\right)\delta d_{AiX} \right) \quad (15)$$

For GF, these coordinates are given by:

$$\delta h_{X\ GF} = \frac{\sum_i \sum_j s_{ji\,X} \left(\mathbf{r}_{ji}^T \delta \mathbf{r}_{ji}\right)}{\sum_i \sum_j s_{ji\,X}^2} \quad (16)$$

$$\delta h_{Y\ GF} = \frac{\sum_i \sum_j s_{ji\,Y} \left(\mathbf{r}_{ji}^T \delta \mathbf{r}_{ji}\right)}{\sum_i \sum_j s_{ji\,Y}^2} \quad (17)$$

2.4. STA compensation by marker cluster 'centering'

Position errors of AoR are adversely affected by the distance between the markers and the axis, in all the methods. This occurs explicitly for GF in the inner product $\mathbf{r}_{ji}^T \delta \mathbf{r}_{ji}$ of Eqs (16-17), which accounts for variations of squared axis-to-marker distances. In MFHA and SARA (13-16), this is implied by the error of the translation parameter at the axis $\left(\delta d_{AiX}, \delta d_{AiY}\right)$, which contains a component proportional to the product

between rotation errors and axis-to-marker distances, such as $\delta\mathbf{q}_{iv}$ and $\mathbf{p}_0$ in the equation for time-variable FHA (2). Accordingly, a potentially effective strategy to reduce AoR position errors may be by using a 'centred' subset of markers, as near to the AoR as possible. In MFHA and SARA, which use pre-calculated rotations and translations as inputs, such 'centering' may be applied to the measurement of translations alone, while using a greater set of markers to calculate the amount of rotation and the direction of the AoR; we call this strategy 'translation-centering' in the remaining of the paper.

2.5 Experimental validation

To validate the equations presented in the previous sections and analyse the efficacy of STA-compensation strategies, we have used a measurement of one healthy subject (male, BMI=27.1) performing a sit-to-stand gesture, previously published by Tsai et al. (Tsai et al., 2009). The data set included the motion of femur and tibia, measured by videofluoroscopy, and the trajectories of 6 skin markers on the thigh (figure 2) and 4 markers on the shank, expressed in the anatomical frames of their respective bones. Thigh markers were displaced between 12.7 and 23.8 mm from their average position with respect to the underlying bone; these displacements were much smaller for the shank, between 2.3 and 10 mm.

The analysis focused on the thigh, which had the greatest artefacts. The relative motion of the femur w.r.t. the tibia was calculated using the first instant (sitting) as the reference pose. The marker trajectories on the thigh reference frame, superimposed on the bone movement, were used to calculate the relative motion with STA, as in Page et al. (2009). Those rotations and translations, without and with artefact, were used to calculate the FHA at each instant, and to estimate the AoR using SARA. All the results

were calculated in the reference frame of the tibia (Wu et al., 2002), with the origin of coordinates set at the midpoint between the tibial epicondyles.

Since the outcome of MFHA is dependent on the reference pose considered for the calculations, two options were tested: a) using the initial pose as the reference and analysing the *N*-1 remaining poses (MFHA-I); b) the 'widest movements' criterion proposed by Camomilla et al. (2006), whereby *N*-1 pairs of poses are chosen from the *N* observed instants attempting to maximise the rotation angles θ_i (MFHA-W).

The AoR was also estimated by GF using the marker trajectories w.r.t. the tibia, either fixed on the femur as in the first instant (without artefacts) or moving as measured (with artefacts).

Different STA compensation strategies were evaluated in order to compare the angle and position errors of the resulting AoR: a traditional procedure like the 'solidification' method, based on finding a subset of markers and frames containing the least deformed triangle of markers throughout the measurement (Begon and Lacouture, 2005), and the 'centering' strategy presented above (table 1). All calculations were made with GNU Octave (Eaton et al., 2015).

3. Results

3.1. Rotation axes with and without STA

The motion of the bone was an 80º extension accompanied by a small adduction and internal rotation. Due to STA the observed range of rotation was diminished by 20º, and the anterior-posterior projection of the rotation axis was reduced (figure 3).

The AoR calculated without STA by MFHA (both variants), SARA and GF were within a distance of less than 4 mm of each other, around 31 mm behind and 60 mm above the tibial epicondyles. On average, the AoR calculated without STA had a projection of 12.3º and 7.5º in the anterior-posterior and vertical directions, respectively.

STA caused a change in the position of the FHA and the AoR calculated by MFHA and SARA of 20 mm (anterior-posterior) to 30 mm (vertical). With GF, the anterior-posterior displacement of the AoR was similar, but it was reduced to 18 mm vertically (figure 4a). The orientation error of the FHA was around 5º for joint rotations over 15º, although it increased to 15º at the smallest angles.

3.2. Measured and estimated errors

For rotation angles over 15º, the estimated errors of the FHA orientation and position according to (1-3) were within 1.6º and 8 mm of the measured errors (figure 5). The differences between measured and estimated errors in AoR position and orientation (table 2) were 7.3 mm on average for the position coordinates (31% of the error size), and 1.5º for the orientation (the same order of magnitude as the error itself).

3.3. Compensation strategies

Table 3 shows the size of AoR position and orientation errors for the different combinations of calculation algorithms and compensation strategies. All the transformation techniques gave similar results, although MFHA-I provided a small advantage. GF gave the smallest orientation and position errors with the default calculations, around 1º and 5-10 mm less than transformation techniques. The opposite was so with the solidification strategy, which hardly changed the results of transformation techniques, but increased the error with GF. Centering the marker cluster was successful for certain combinations: it reduced orientation errors in MFHA/SARA,

and position errors in GF. MFHA/SARA position errors were also considerably reduced with the specific 'translation-centering' strategy (figure 4b).

4. Discussion

We have presented a mathematical model of the propagation of STA to the position and direction of variable FHA and fixed AoR, as calculated by three functional calibration techniques: MFHA, SARA and GF; and we have also explored the potential effectiveness of STA-compensation strategies in light of the resulting equations and *in-vivo* knee data from a published study. Without STA-compensation, all methods yielded errors of less than 3º in the orientation of the AoR and between 30 and 40 mm in its position, which were predicted by the models within 1.5º and 7.3 mm on average. STA-compensation strategies had diverse effects on each functional calibration technique.

The differences observed between methods may be related to the variety of published results. Only two studies made *in-vivo* comparisons between methods: Van Campen et al. (2011) reported more accurate estimates of the AoR for GF with five healthy subjects performing isokinetic knee flexion-extension, whereas Colle et al. (2016) reported that SARA achieved better estimates for 106 subjects with surgical implants, during passive knee flexion-extension. In both cases the reported differences focused on AoR orientation errors. Without STA-compensation, we obtained better results using GF, for both AoR orientation and location. In this regard, it should be noted that the sit-to-stand gesture that we analysed was unlike any of those studies: the joint motion was mainly driven by a movement of the thigh while the shank stood with constant foot support, and thigh markers were atypically distributed, all relatively close to the knee to keep them in the field of view of the fluoroscopy system.

Transformation techniques gave results that were similar to each other in all circumstances. An advantage of SARA is that it originally considers two moving segments and is independent of any relative reference pose. MFHA can work around that problem by using all pairs of observed postures (Schwartz and Rozumalski, 2005), which gives identical results to SARA (Ehrig et al., 2007). Instead of all pairs, we used the 'widest movements' criterion, which is computationally more efficient (Camomilla et al., 2006), and it also gave results that were virtually identical to SARA. But unexpectedly, a naïver approach using the initial observation as the common reference posture (MFHA-I) gave systematically smaller position errors (3.4 mm closer to the 'true' AoR on average), although choosing other initial positions might not provide the same benefit.

This implies that, unlike in the case of random errors, maximizing rotation angles does not guarantee that the effect of STA is minimised, insofar as the size of the errors increases with the rotation itself. It remains to be studied what the optimal tradeoff may be between information given by large rotations and error introduced by increased artefacts.

STA-compensation strategies showed varied performance. The aim of solidification is to reduce errors deriving from the deformation associated with STA (Chèze et al., 1995). However, the error equations that we derived do not show direct effects of errors in inter-marker distances. In the experiment, solidification left the results unchanged (for MFHA and SARA) or even increased the error (GF).

That failure of solidification has been previously reported, because the main component of STA is a rigid movement of muscle and fat masses over the bone, so minimizing deformations often changes little (Andersen et al., 2012; Bonci et al., 2015; Camomilla

et al., 2015; De Rosario et al., 2012; Dumas et al., 2015). When STA mainly consist of such rigid movement of the entire cluster, any analysis that only considers rigid motion may be expected not to be very sensitive to solidification, as we observed with transformation techniques. GF, which does account for deformations, was negatively influenced by solidification, although this result is more difficult to extrapolate to other experimental configurations, since other factors like the distribution of markers and the range of movement also greatly influence GF equations.

The 'centering' strategy of selecting a subset of markers near to the axis was posited due to the influence of markers-to-axis distance on errors observed in the equations. Since we only had one measurement with a fixed marker distribution, we attempted this 'centering' by selecting the subset of three markers closest to the joint. Using that reduced marker set for the whole analysis was only slightly beneficial for GF, but not for transformation techniques. This may be partially explained by the fact that in GF, axis-to-marker distances amplify the error of each individual marker; however, in transformation techniques the main effect of that distance is to amplify the rotation error, but narrowing the distribution of markers is detrimental for the accurate measurement of the rotation itself (Crisco III et al., 1994), so the benefit of using only centred markers is not obvious.

On the other hand, an advantage of transformation techniques is that their equations have two inputs — rotation and translation parameters — that can be obtained from separate marker groups. That is the basis of the 'translation-centering' strategy, which reduced the position error to around 40% of its original value. This is a promising result, although it may be conditioned by the specific configuration of the markers in the data

set. For other kinematic analyses and marker distributions, placing markers away from the axis may give better results (Kratzenstein et al., 2012).

Partial knowledge of the relative size and direction of STA in different skin regions (Fukui et al., 2016; Stagni et al., 2005) might also be used to design marker clusters that avoid problematic areas, since not all artefacts have the same impact. This is particularly clear for the GF method, since marker position errors appear explicitly in the AoR error formulas.

This study was limited to one sample case, and the analysis was restricted to the motion of the thigh marker cluster, relative to the error-free reference frame of the tibia. This was done for the sake of clarity in the formulas, although it is a simplification of the reality. The artefacts of shank markers were much smaller, but not negligible, and adding them may increase the errors for all methods, although perhaps not in the same proportion. SARA is the only method whose original formulation accounts for the motion of both segments, and it might have shown better performance in that situation.

Finally, the validity of the fixed axis model should be discussed. It is a common assumption for the knee joint (Clément et al., 2015; Stagni et al., 2009), although in other works it is recommended that more complex models should be used (Clément et al., 2014; Duprey et al., 2010; Gasparutto et al., 2015). Ruling out the observations with rotations of less than 10º, the deviation of the FHA based on bone measures was sufficiently small as to be negligible with respect to STA, but the axis was not absolutely fixed. So other models might be explored, although others have found a limited efficacy of imposing complex kinematic constraints on joint axes, in order to control STA (Andersen et al., 2010).

In conclusion, no functional calibration technique was shown to be generally superior to others regarding the impact of STA. The error equations and experimental results obtained with a sample data set showed that the performance of each technique depends on different characteristics of the artefacts, and suggest different strategies to compensate for them. GF may be better suited to measures where it is possible to minimize the displacement of the markers in the direction that separates them from the AoR, whereas transformation techniques may take advantage of separate estimations of the marker cluster rotations and translations. These suggestions should be experimentally contrasted with more varied examples of marker distributions and joint movements.

Acknowledgements

This work was funded by the Spanish Government and co-financed by EU FEDER funds (Grant DPI2013-44227-R). We would like to thank Prof. Tung-Wu Lu, Tsung-Yuan Tsai, Mei-Ying Kuo and Horn-Chaung Hsu from National Taiwan University for making the data from their studies available for further research on STA, and Dr. Tecla Bonci from the Italian University of Sport and Movement 'Foro Italico' for providing the access to benchmark data.

Conflict of interest statement

The authors of this paper declare that they do not have any conflict of interest related to the purpose.

References

Andersen, M.S., Benoit, D.L., Damsgaard, M., Ramsey, D.K., Rasmussen, J., 2010. Do kinematic models reduce the effects of soft tissue artefacts in skin marker-based motion analysis? An in vivo study of knee kinematics. Journal of Biomechanics 43, 268–273. doi:10.1016/j.jbiomech.2009.08.034

Andersen, M.S., Damsgaard, M., Rasmussen, J., Ramsey, D.K., Benoit, D.L., 2012. A linear soft tissue artefact model for human movement analysis: Proof of concept using in vivo data. Gait & Posture 35, 606–611. doi:10.1016/j.gaitpost.2011.11.032

Begon, M., Lacouture, P., 2005. Solidification procedure adapted to locating joint centre. Computer Methods in Biomechanics and Biomedical Engineering 8, 23–24. doi:10.1080/10255840512331880074

Besier, T.F., Sturnieks, D.L., Alderson, J.A., Lloyd, D.G., 2003. Repeatability of gait data using a functional hip joint centre and a mean helical knee axis. Journal of Biomechanics 36, 1159–1168. doi:10.1016/S0021-9290(03)00087-3

Bonci, T., Camomilla, V., Dumas, R., Chèze, L., Cappozzo, A., 2015. Rigid and non-rigid geometrical transformations of a marker-cluster and their impact on bone-pose estimation. Journal of Biomechanics 48, 4166–4172. doi:10.1016/j.jbiomech.2015.10.031

Camomilla, V., Bonci, T., Dumas, R., Chèze, L., Cappozzo, A., 2015. A model of the soft tissue artefact rigid component. Journal of Biomechanics 48, 1752–1759. doi:10.1016/j.jbiomech.2015.05.007

Camomilla, V., Cereatti, A., Vannozzi, G., Cappozzo, A., 2006. An optimized protocol for hip joint centre determination using the functional method. Journal of Biomechanics 39, 1096–1106. doi:10.1016/j.jbiomech.2005.02.008

Chèze, L., Fregly, B.J., Dimnet, J., 1995. A solidification procedure to facilitate kinematic analyses based on video system data. Journal of Biomechanics 28, 879–884. doi:16/0021-9290(95)95278-D

Clément, J., Dumas, R., Hagemeister, N., de Guise, J.A., 2015. Soft tissue artifact compensation in knee kinematics by multi-body optimization: Performance of subject-specific knee joint models. Journal of Biomechanics 48, 3796–3802. doi:10.1016/j.jbiomech.2015.09.040

Clément, J., Hagemeister, N., Dumas, R., Kanhonou, M., Guise, J.A. de, 2014. Influence of biomechanical multi-joint models used in global optimisation to estimate healthy and osteoarthritis knee kinematics. Computer Methods in Biomechanics and Biomedical Engineering 17, 76–77. doi:10.1080/10255842.2014.931141

Colle, F., Lopomo, N., Visani, A., Zaffagnini, S., Marcacci, M., 2016. Comparison of three formal methods used to estimate the functional axis of rotation: an extensive in-vivo analysis performed on the knee joint. Computer Methods in Biomechanics and Biomedical Engineering 19, 484–492. doi:10.1080/10255842.2015.1042464

Crisco III, J.J., Chen, X., Panjabi, M.M., Wolfe, S.W., 1994. Optimal marker placement for calculating the instantaneous center of rotation. Journal of Biomechanics 27, 1183–1187. doi:10.1016/0021-9290(94)90059-0

De Rosario, H., Page, A., Besa, A., Mata, V., Conejero, E., 2012. Kinematic description of soft tissue artifacts: quantifying rigid versus deformation components and

their relation with bone motion. Med Biol Eng Comput 50, 1173–1181. doi:10.1007/s11517-012-0978-5

De Rosario, H., Page, Á., Besa, A., Valera, Á., 2013. Propagation of soft tissue artifacts to the center of rotation: A model for the correction of functional calibration techniques. Journal of Biomechanics 46, 2619–2625. doi:10.1016/j.jbiomech.2013.08.006

Della Croce, U., Leardini, A., Chiari, L., Cappozzo, A., 2005. Human movement analysis using stereophotogrammetry: Part 4: assessment of anatomical landmark misplacement and its effects on joint kinematics. Gait & posture 21, 226–237.

Dumas, R., Camomilla, V., Bonci, T., Chèze, L., Cappozzo, A., 2015. What Portion of the Soft Tissue Artefact Requires Compensation When Estimating Joint Kinematics? J Biomech Eng 137, 064502–064502. doi:10.1115/1.4030363

Duprey, S., Cheze, L., Dumas, R., 2010. Influence of joint constraints on lower limb kinematics estimation from skin markers using global optimization. Journal of Biomechanics 43, 2858–2862. doi:10.1016/j.jbiomech.2010.06.010

Eaton, J.W., Bateman, D., Hauberg, S., Wehbring, R., 2015. GNU Octave version 4.0.0 manual: a high-level interactive language for numerical computations.

Ehrig, R.M., Taylor, W.R., Duda, G.N., Heller, M.O., 2007. A survey of formal methods for determining functional joint axes. Journal of Biomechanics 40, 2150–2157. doi:10.1016/j.jbiomech.2006.10.026

Fukui, T., Otake, Y., Kondo, T., 2016. In which direction does skin move during joint movement? Skin Res Technol 22, 181–188. doi:10.1111/srt.12248

Gamage, S.S.H.U., Lasenby, J., 2002. New least squares solutions for estimating the average centre of rotation and the axis of rotation. Journal of Biomechanics 35, 87–93. doi:10.1016/S0021-9290(01)00160-9

Gasparutto, X., Sancisi, N., Jacquelin, E., Parenti-Castelli, V., Dumas, R., 2015. Validation of a multi-body optimization with knee kinematic models including ligament constraints. Journal of Biomechanics 48, 1141–1146. doi:10.1016/j.jbiomech.2015.01.010

Halvorsen, K., Lesser, M., Lundberg, A., 1999. A new method for estimating the axis of rotation and the center of rotation. Journal of Biomechanics 32, 1221–1227. doi:10.1016/S0021-9290(99)00120-7

Kratzenstein, S., Kornaropoulos, E.I., Ehrig, R.M., Heller, M.O., Pöpplau, B.M., Taylor, W.R., 2012. Effective marker placement for functional identification of the centre of rotation at the hip. Gait & Posture 36, 482–486. doi:10.1016/j.gaitpost.2012.04.011

Lin, C.-C., Lu, T.-W., Lu, H.-L., Kuo, M.-Y., Hsu, H.-C., 2016. Effects of soft tissue artifacts on differentiating kinematic differences between natural and replaced knee joints during functional activity. Gait & Posture 46, 154–160. doi:10.1016/j.gaitpost.2016.03.006

MacWilliams, B.A., 2008. A comparison of four functional methods to determine centers and axes of rotations. Gait & Posture 28, 673–679. doi:10.1016/j.gaitpost.2008.05.010

Page, A., Rosario, H. de, Mata, V., Atienza, C., 2009. Experimental Analysis of Rigid Body Motion. A Vector Method to Determine Finite and Infinitesimal Displacements From Point Coordinates. Journal of Mechanical Design 131, 031005.

Reichl, I., Ongaro, M., 2013. Finite helical axis versus symmetrical axis of rotation approach for the human knee joint: squats, rowing and cycling. Computer Methods in Biomechanics and Biomedical Engineering 16, 109–111. doi:10.1080/10255842.2013.815943

Schwartz, M.H., Rozumalski, A., 2005. A new method for estimating joint parameters from motion data. Journal of Biomechanics 38, 107–116. doi:10.1016/j.jbiomech.2004.03.009

Stagni, R., Fantozzi, S., Cappello, A., 2009. Double calibration vs. global optimisation: Performance and effectiveness for clinical application. Gait & posture 29, 119–122.

Stagni, R., Fantozzi, S., Cappello, A., Leardini, A., 2005. Quantification of soft tissue artefact in motion analysis by combining 3D fluoroscopy and stereophotogrammetry: a study on two subjects. Clinical Biomechanics 20, 320–329. doi:10.1016/j.clinbiomech.2004.11.012

Tsai, T.-Y., Lu, T.-W., Kuo, M.-Y., Hsu, H.-C., 2009. Quantification of three-dimensional movement of skin markers relative to the underlying bones during functional activities. Biomed. Eng. Appl. Basis Commun. 21, 223–232. doi:10.4015/S1016237209001283

Van Campen, A., De Groote, F., Bosmans, L., Scheys, L., Jonkers, I., De Schutter, J., 2011. Functional knee axis based on isokinetic dynamometry data: Comparison of two methods, MRI validation, and effect on knee joint kinematics. Journal of Biomechanics 44, 2595–2600. doi:10.1016/j.jbiomech.2011.08.022

Woltring, H.J., 1990. Data processing and error analysis, in: Cappozzo, A., Berme, P. (Eds.), Biomechanics of Human Movement: Applications in Rehabilitation, Sport and Ergonomics. Bertec Corporation, Worthington, OH, pp. 203–227.

Wu, G., Siegler, S., Allard, P., Kirtley, C., Leardini, A., Rosenbaum, D., Whittle, M., D'Lima, D.D., Cristofolini, L., Witte, H., Schmid, O., Stokes, I., 2002. ISB recommendation on definitions of joint coordinate system of various joints for the reporting of human joint motion—part I: ankle, hip, and spine. Journal of Biomechanics 35, 543–548. doi:10.1016/S0021-9290(01)00222-6

List of figures

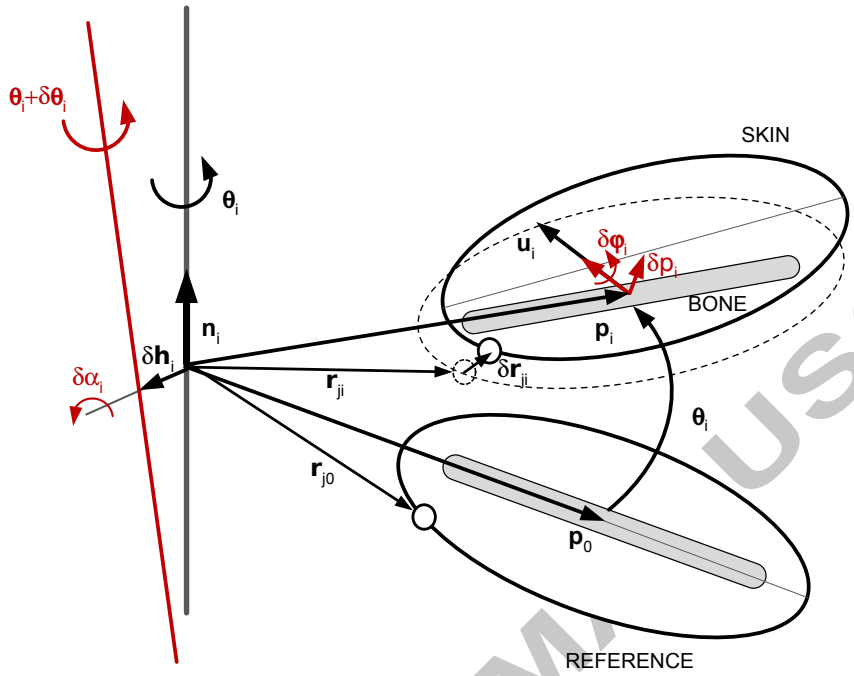

Figure 1. Schematic representation of the STA and its effect on the FHA. The bone rotates at an angle θ_i around the FHA from a reference pose to its pose at time t_i, such that any arbitrary point $\mathbf{p}_0$ of the body moves to $\mathbf{p}_i$. The group markers on the skin ($\mathbf{r}_{ji}$) undergo a displacement over the bone ($\delta\mathbf{r}_{ji}$), consisting of a deformation and a rigid motion of the entire marker cluster. That rigid motion can be described by a rotation $\delta\varphi_i$ around the axis $\mathbf{u}_i$, and a translation $\delta\mathbf{p}_i$ added to $\mathbf{p}_i$. As a result, there is a variation $\delta\theta_i$ in the rotation angle, while the FHA is deviated at an angle $\delta\alpha_i$ from its original direction, and displaced by a distance $\delta\mathbf{h}_i$.

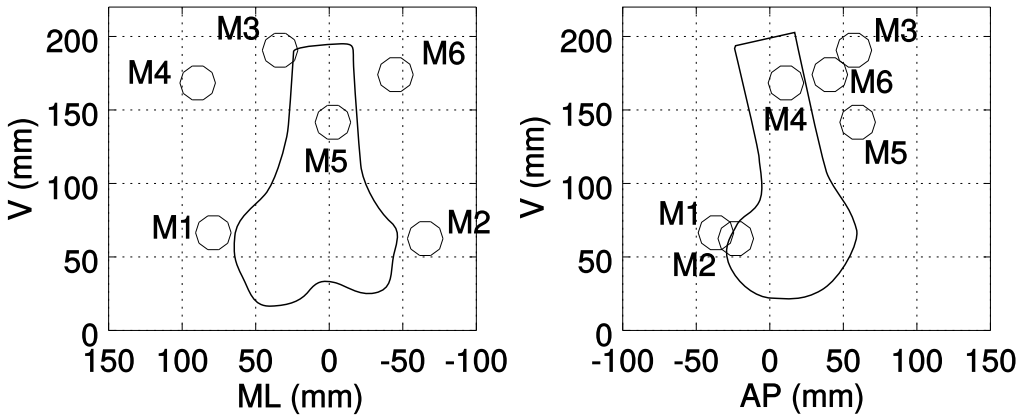

Figure 2. Frontal and lateral views of the distribution of thigh markers, with a figurative representation of the femur. Their positions are expressed in the coordinate system of the tibia in the standing position, according to Wu et al. (2002), with the origin set at the midpoint between tibial epicondyles. AP: anterior-posterior axis of the tibia, pointing anteriorly; ML: medial-lateral axis of the tibia, pointing laterally; V: vertical axis of the tibia.

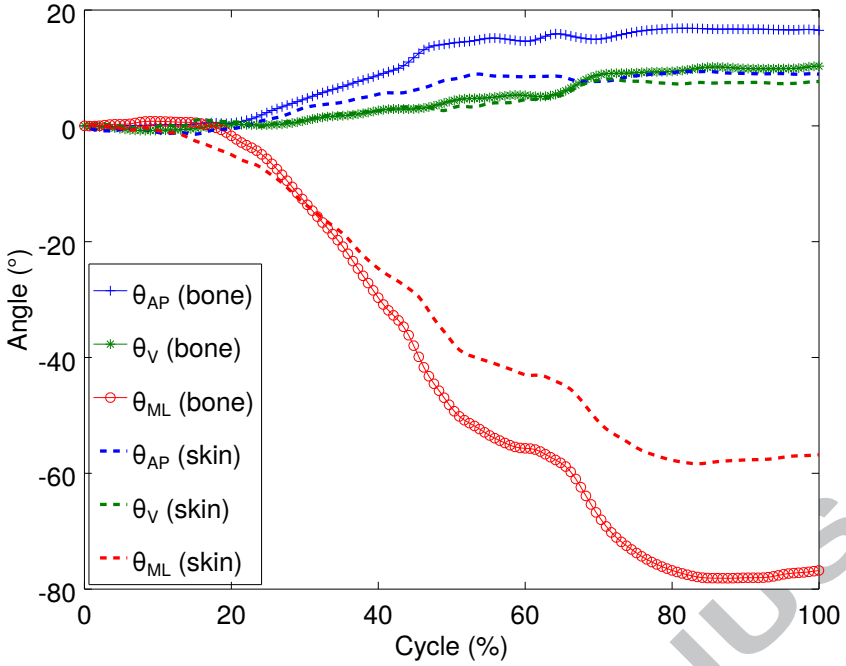

Figure 3. Projections of the attitude vector $\theta_i \delta \mathbf{u}_i$ on the anatomical axes of the tibia.

(AP: anterior-posterior axis, V: vertical axis, ML: medial-lateral axis).

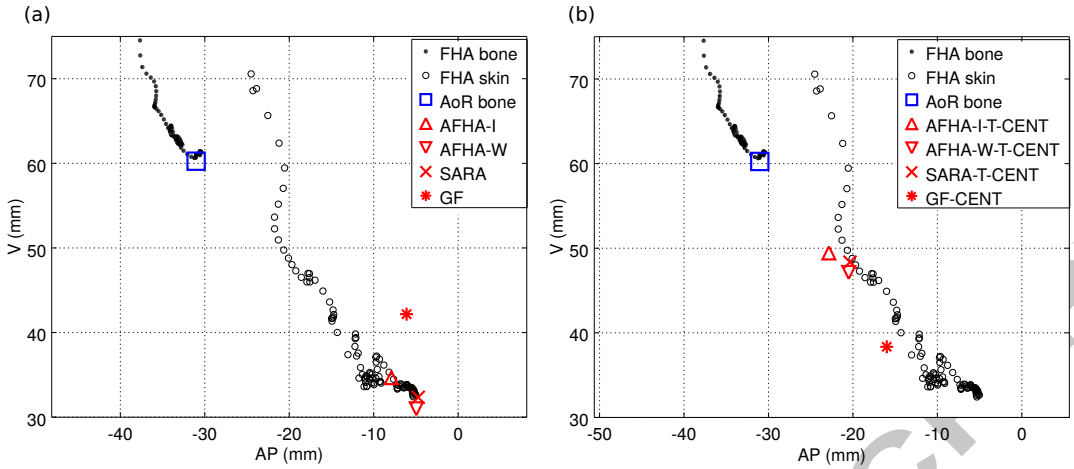

Figure 4. Sagittal projection of variable FHA and fixed AoR calculated with the different methods, for the bone motion and skin motion with STA. The AoR shown for the bone is the average of the four methods (MFHA-I, MFHA-W, SARA, and GF). (a): Default strategy, without error compensation. (b) Best result with the different compensation strategies.

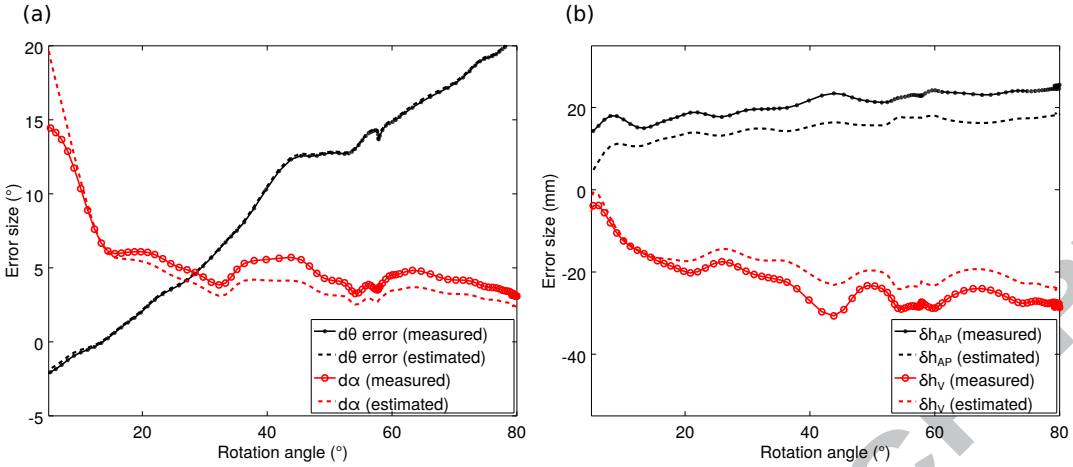

Figure 5. Measured and estimated errors for the variable FHA. (a) Error in the magnitude of rotation ($\delta\theta_i$) and angle between the real and observed FHA ($\delta\alpha_i$). (b) Error in the position of the FHA projected on the anterior-posterior axis (AP, pointing anteriorly) and the vertical axis (V, pointing upwards).

List of tables

Table 1. Combinations of methods used to calculate AoR parameters.

Abbreviation	Description of the strategy	Applied methods
DEF	Default calculations with all markers	MFHA-I, MFHA-W, SARA, GF
SOL-100	Solidification with 100% of frames	MFHA-I, MFHA-W, SARA, GF
SOL-80	Solidification with 80% of least-deformed frames	MFHA-I, MFHA-W, SARA, GF
CENT	Using the three markers closest to the knee joint (M1, M2, M5)	MFHA-I, MFHA-W, SARA, GF
T-CENT	Using all markers to determine the rotation of the joint, but only the three closest to the joint (M1, M2, M5) to determine the translation	MFHA-I, MFHA-W, SARA

Table 2. AoR position and orientation errors, expressed in the anatomical axes of the tibia (AP: anterior-posterior axis, pointing anteriorly, V: vertical, axis, pointing upwards).

		Position error (mm)		Orientation error (º)	
		$\delta \mathbf{h}_{AP}$	$\delta \mathbf{h}_{V}$	$\delta \alpha_{AP}$	$\delta \alpha_{V}$
MFHA-I	Measured	23.1	-25.6	0.6	2.6
	Estimated	21.3	-17.8	1.7	2.0
MFHA-W	Measured	26.1	-29.3	0.3	2.6
	Estimated	14.9	-24.7	-1.2	1.3
SARA	Measured	26.3	-27.9	1.0	2.4
	Estimated	20.3	-17.7	2.0	3.2
GF	Measured	24.9	-18.1	0.9	1.5
	Estimated	32.3	-27.4	-3.3	-0.0

Table 3. AoR position and orientation errors, using different combinations of AoR calculation methods and error compensation strategies.

	Position error (mm)				Orientation error (º)			
	MFHA-I	MFHA-W	SARA	GF	MFHA-I	MFHA-W	SARA	GF
DEF	34.5	39.2	38.4	30.9	2.7	2.7	2.5	1.8
SOL-100	33.5	37.8	36.7	39.3	2.8	2.8	2.5	2.2
SOL-80	33.6	40.8	39.1	42.4	2.8	3.5	3.4	3.4
CENT	35.2	37.5	37.2	26.5	1.4	1.0	0.4	1.9
T-CENT	13.5	16.8	16.0					